forests

MDPI

Article

Study on the Shear Strength of Root-Soil Composite and Root Reinforcement Mechanism

Pengcheng Li [1], Xuepei Xiao [2,*], Lizhou Wu [3], Xu Li [4], Hong Zhang [3,*] and Jianting Zhou [3]

[1] School of Environment and Civil Engineering, Chengdu University of Technology, Chengdu 610059, China; lipengcheng970507@163.com
[2] Sichuan Highway Planning, Survey, Design and Research Institute Ltd., Chengdu 610041, China
[3] State Key Laboratory of Mountain Bridge and Tunnel Engineering, Chongqing Jiaotong University, Chongqing 400074, China; lzwu@cqjtu.edu.cn (L.W.); jtzhou@cqjtu.edu.cn (J.Z.)
[4] Key Laboratory of Urban Underground Engineering, Ministry of Education, Beijing Jiaotong University, Beijing 100044, China; cexuli2012@163.com
* Correspondence: xiaoxuepei@schdri.com (X.X.); hongzhang@cqjtu.edu.cn (H.Z.)

Abstract: This study investigates the effects of root distributions and stress paths on the shear strength of root-soil composites using a consolidated-undrained (CU) triaxial test. On the basis of the limit equilibrium, two root reinforcement coefficients (n and m) are proposed for characterizing the effects of shear strength parameters on the principal stress considering different root distribution angles and root diameters. Then, n and m are introduced into the conventional limit equilibrium equation to develop a new limit equilibrium equation for root-soil composites. The results demonstrate that the root distribution angles (α) and root diameters (d) affect the shear strength of the root-soil composites. Under a consolidated-undrained condition, the effective cohesion (c'_{rs}) of the rooted soil is high and decreases in the order of 90°, 0°, 30° and 60°. For the same root distribution angle, c'_{rs} increases with the increasing root diameter. Meanwhile, the effective internal friction angle (φ'_{rs}) changes slightly. The failure principal stress of the root-soil composites is positively correlated with n and m. Furthermore, the deformation of the samples indicates that the run-through rate of α = 90° and α = 0° are both 0. Meanwhile, the lateral deformation rate declines from 17.0% for α = 60° to 10.9% for α = 90°.

Keywords: root-soil composite; root reinforcement coefficient; shear strength parameters; root distribution angle; root diameter

Citation: Li, P.; Xiao, X.; Wu, L.; Li, X.; Zhang, H.; Zhou, J. Study on the Shear Strength of Root-Soil Composite and Root Reinforcement Mechanism. *Forests* **2022**, *13*, 898. https://doi.org/10.3390/f13060898

Academic Editors: Haijia Wen, Weile Li, Chong Xu and Hiromu Daimaru

Received: 8 May 2022
Accepted: 6 June 2022
Published: 9 June 2022

1. Introduction

Landsliding is a geological disaster which occurs around the world and poses a great threat to people's lives and property [1–7]. Plant roots play an important role in stabilizing shallow slopes [8,9]. In recent years, vegetation has been widely used in ecological engineering to prevent soil erosion and stabilize slopes effectively [10–14].

Two mechanisms by which vegetation affects slope stability are recognized: (a) the mechanical reinforcement of the soil by plant roots and (b) the improvement of the hydrological conditions of slopes [15–18]. Plant transpiration affects soil matric suction [19,20], while plant roots absorb water and reduce the pore water pressure [21,22], and the mechanical reinforcement of plant roots has been proposed [23]. The most important contribution of roots is their ability to increase the shear strength of soils. Strong frictional properties of the root-soil interface improve the stability of the root-soil composites [24]. Additionally, the reinforcement effect of roots is represented in the increment of the shear strength of root-soil composites compared with that of unreinforced soil [25]. Many field and laboratory tests have been conducted and mechanical models of root-soil composites, including the Wu-Waldron model, modified Wu-Waldron model, root bundle model, and fiber bundle model, have been developed [26–31]. Rahardjo et al. [32], and Satyanaga and Rahardjo [33]

investigated the effect of plant roots on slope stability under unsaturated conditions using undisturbed soil with and without roots. Triaxial tests were conducted to investigate the mechanical properties of reinforced and unreinforced soils. Zhang et al. [25] carried out a series of consolidated drained triaxial tests to examine the influence of roots on the shear strength of soils. Zhou and Wang [34] further showed that the shear strength of root-soil composites is higher than that of unreinforced soil.

At present, most researchers studied the effect of roots on the shear strength of rooted soils mainly based on the root content, root distribution pattern (usually horizontal and vertical), and moisture content [35–38]. Unfortunately, except for the influence of horizontal and vertical distribution patterns of roots on the strength of rooted soils, the reinforcement effect of other root distribution angles on root-soil composites has rarely been mentioned. Plant roots freely grow at an angle in the soils and the diameters of roots constantly change. Furthermore, the changes in the shear strength influence the failure principal stress of rooted soils, but the limit equilibrium equation for the failure principal stress of rooted soils has not been developed. Therefore, it is necessary to analyze the influence of root distribution angles and root diameters on the shear strength of root-soil composites. Moreover, the limit equilibrium equation of root-soil composites needs to be developed to investigate the impact of shear strength parameters on the failure principal stress of root-soil composites.

This study aims to examine the effect of root distribution angles (α = 0°, 30°, 60°, and 90°) and root diameters (d = 0.5 mm, 1.0 mm, and 2.0 mm) on the shear strength of soils. Based on the conventional limit equilibrium equation, two root reinforcement coefficients (n and m) are proposed to describe the influence of the variations of an effective internal friction angle and effective cohesion on the failure principal stress of root-soil composites, respectively. A new limit equilibrium equation of root-soil composites is then developed. Additionally, the deformation of soil samples is examined to demonstrate the constraint effect of roots on soils. The results provide a new insight for the analysis of the shear strength of rooted soils and provide a reference for choosing suitable slope protection plants.

2. Materials and Experimental Methods

2.1. Experimental Materials

The soils were obtained from Beijing, China (about 40°28′ N, 115°58′ E). Sieving method was used in the particle analysis test. The particle size distribution of the tested soils is shown in Figure 1 and Table 1. The soil is well-graded sand with clay and gravel (SW-SC) according to the unified soil classification system (USCS) [39] and its basic physical properties [40,41] are shown in Table 2.

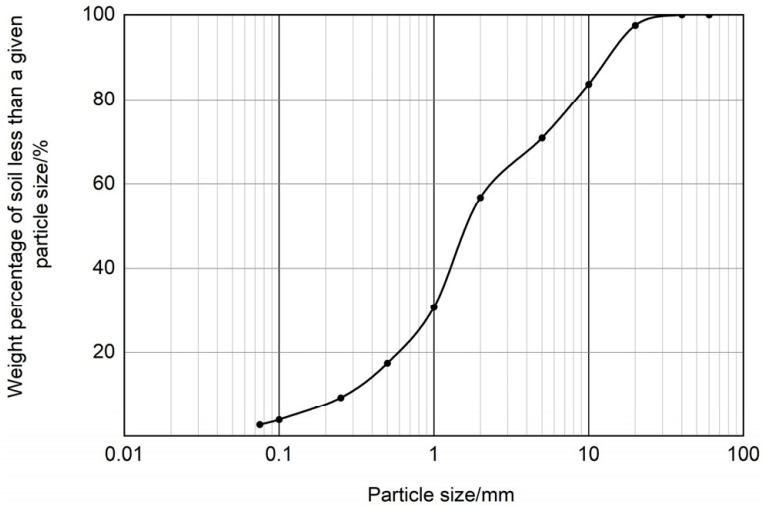

Figure 1. Particle size distribution curve of the tested soils.

Table 1. Particle size distribution of the tested soils.

Particle Size/mm	>10	10–5	5–2	2–1	1–0.5	0.5–0.25	0.25–0.075	≤0.075
Percentage/%	16.3	12.8	14.2	25.97	13.3	8.23	6.5	2.7

Table 2. Physical properties of the tested soils.

Soil Dry Density (kg/m^3)	Water Content (%)	Plastic Limit (%)	Liquid Limit (%)	Plasticity Index	Specific Gravity	Unified Soil Classification System, USCS
1800	16.5	15.2	30.7	15.5	2.73	Well-graded sand with clay and gravel (SW-SC)

Pyracantha fortuneana (Maxim.) Li, an evergreen shrub, is a commonly used plant for soil and water conservation and was chosen as the experimental root system. Fifty *Pyracantha fortuneana* plants (about 80–90 cm in height) were wholly excavated and the root diameters and distribution angles were counted. A total of 200 roots were measured using vernier caliper. The root diameters ranged from 0.5 mm to 4.5 mm and were mainly distributed within 0.5 mm to 2.0 mm. Moreover, roots were widely distributed in the depth of 0.5 m below the surface and the distribution angles of roots were 0°, 30°, 60°, and 90°. Root architecture of *Pyracantha fortuneana* was horizontal [42]. In the tests, the root lengths were 30.0 and 60.0 mm and the diameters were 0.5, 1.0, and 2.0 mm, respectively. In Figure 2a–c, twelve roots with a length of 30.0 mm were set in three layers in a sample, and four roots were evenly placed in each layer. In Figure 2d, six roots with 60.0 mm length were evenly distributed in the sample. The root content of all the samples was 0.15%.

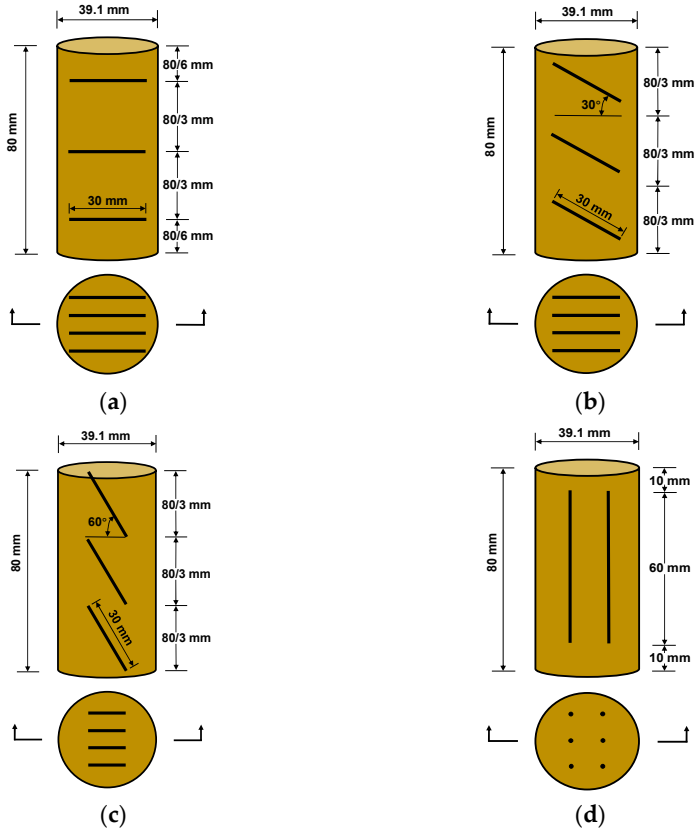

Figure 2. Diagram of the root distribution angles in the triaxial test: (**a**) 0°, (**b**) 30°, (**c**) 60°, (**d**) 90°.

2.2. Experimental Methods

Below the surface depth of 0.5 m, the enhancement effect of roots on the soil strength will be greatly weakened with the decrease of the number of roots. Therefore, the confining pressures (50 kPa, 100 kPa, and 150 kPa) were chosen to effectively evaluate the influence of roots on the soil strength. To study the influence of root distribution angles on soil strength, four root distribution angles (0°, 30°, 60°, and 90°, respectively) were employed and the root distribution patterns are shown in Figure 2.

Slope soils have generally reached a consolidated state under natural conditions. Slope instability caused by soil erosion is usually represented by the rapid increase of pore water pressure within a short time, resulting in a great decrease in soil strength under undrained condition [36]. Therefore, the consolidation undrained (CU) triaxial test was used to investigate the stress-strain response of soils using the TSZ strain-controlled automatic triaxial apparatus (control precision is ±1%). The soil samples are saturated by vacuum saturation method. The dry density and moisture content of the soils are 1800 kg/m^3 and 16.5%, respectively. The samples with 16.5% moisture content were prepared using three-layer compaction method. The samples of the root-soil composites and the unreinforced soils were 39.1 mm in diameter and 80.0 mm in height.

The range of shearing rate of TSZ was 0.002–4 mm/min ± 10%. The shearing rate of the triaxial tests was chosen as 0.1 mm/min and the stress was recorded every 0.1% increase of axial strain. When the strain reached 20%, the test ended. The mean values of the test results of effective stress were taken as the final values of deviator stress. The maximum deviator stress was taken as the failure stress. However, when the peak value of deviator stress was not recorded, the deviator stress corresponding to 15% strain was taken as the failure stress.

As for unreinforced soils, root-soil composites conform to the Mohr-Coulomb theory [27]. The shear strength of unreinforced soils and root-soil composites is rewritten as [43]:

$$\tau_f = c' + (\sigma - u)\tan\varphi' = c' + \sigma'\tan\varphi' \quad (1)$$

where τ_f is the shear strength (kPa); σ represents the normal stress (kPa); u is the pore water pressure (kPa); σ' is the effective stress (kPa); and c' and φ' represent the effective cohesion (kPa) and the effective internal friction angle (°), respectively.

3. Limit Equilibrium Equation of Root-Soil Composites

Previous studies showed that plant roots can reinforce soils [44] and shear strength parameters of root-soil composites are different from those of unreinforced soils. The limit equilibrium equations of unreinforced soil and root-soil composite are:

$$\sigma_1 = \sigma_3 K_p + 2c'_{us}\sqrt{K_p} \quad (2)$$

$$\sigma_{1l} = \sigma_3 K_{pl} + 2c'_{rs}\sqrt{K_{pl}} \quad (3)$$

where σ_1 and σ_{1l} represent the failure principal stress (kPa) of the unreinforced soil and root-soil composite under confining pressure σ_3, respectively; $K_p = \tan^2\left(45^\circ + \varphi'_{us}/2\right)$ is the passive earth pressure coefficient of the unreinforced soil; $K_{pl} = \tan^2\left(45^\circ + \varphi'_{rs}/2\right)$ is the passive earth pressure coefficient of the root-soil composite; and c'_{us}, φ'_{us}, c'_{rs}, and φ'_{rs} are the effective cohesion (kPa) and effective internal frictional angle (°) of the unreinforced soil and root-soil composites, respectively.

Under the same confining pressure (σ_3), the deviator of the failure principal stress of the unreinforced soil and root-soil composite is given by:

$$\Delta\sigma_{1l} = \sigma_{1l} - \sigma_1 \quad (4)$$

The limit equilibrium equation of the root-soil composite can also be written using the generalized equivalent confining pressure [37]:

$$\sigma_{1l} = (\sigma_3 + \Delta\sigma_{3g})K_p + 2c'_{us}\sqrt{K_p} = \sigma_1 + \Delta\sigma_{3g}K_p \quad (5)$$

where $\Delta\sigma_{3g}$ is the generalized equivalent confining pressure (kPa), which means the difference of confining pressure between unreinforced soil and root-soil composite samples under the same shear strength.

The generalized equivalent confining pressure is written as:

$$\Delta\sigma_{3g} = \frac{\sigma_{1l} - \sigma_1}{K_p} = \frac{\Delta\sigma_{1l}}{K_p} \quad (6)$$

The variations of shear strength parameters in Equation (5) are reflected in the generalized equivalent confining pressure while the variations of the shear strength parameters of Equation (3) are directly reflected in the limit equilibrium equation. Equations (3) and (5) are, therefore, equivalent.

Under the same confining pressure (σ_3), Equations (3) and (5) can be substituted into Equation (4) to obtain the deviator of the failure principal stress of the root-soil composite and the unreinforced soil. $\Delta\sigma_{1l}$ is given by:

$$\Delta\sigma_{1l} = \sigma_3\left(K_{pl} - K_p\right) + 2c'_{us}\left(\sqrt{K_{pl}} - \sqrt{K_p}\right) + 2\left(c'_{rs} - c'_{us}\right)\sqrt{K_{pl}} \quad (7)$$

By substituting Equation (7) into Equation (6), we can gain a new expression of $\Delta\sigma_{3g}$, which is written as:

$$\Delta\sigma_{3g} = \frac{\sigma_3\left(K_{pl} - K_p\right) + 2c'_{us}\left(\sqrt{K_{pl}} - \sqrt{K_p}\right) + 2(c'_{rs} - c'_{us})\left(\sqrt{K_{pl}} - \sqrt{K_p}\right)}{K_p} \quad (8)$$

Substituting Equation (8) into Equation (5), the failure principal stress of the root-soil composite is obtained as:

$$\sigma_{1l} = \sigma_3 K_p \frac{K_{pl}}{K_p} + 2c'_{us}\sqrt{K_p}\left(\sqrt{\frac{K_{pl}}{K_p}} + \frac{c'_{rs} - c'_{us}}{c'_{us}}\sqrt{\frac{K_{pl}}{K_p}}\right) \quad (9)$$

The parameters in Equation (9) are written as:

$$n = \frac{K_{pl}}{K_p} \quad (10)$$

$$m = 1 + \left(\frac{c'_{rs} - c'_{us}}{c'_{us}}\right) \quad (11)$$

where n and m are the root reinforcement coefficients of the soil, which represent the variation of the internal friction angle and cohesion of the rooted soils, respectively.

Equation (9) is, therefore, rewritten as:

$$\sigma_{1l} = n\sigma_3 K_p + 2c'_{us}m\sqrt{n}\sqrt{K_p} \quad (12)$$

Equation (12) is the same as Equation (2) except that the root reinforcement coefficients are introduced into the limit equilibrium equation of the root-soil composite.

4. Results

4.1. Shear Strength Parameters of Root-Soil Composites

Table 3 lists the effects of the root distribution angles and diameters on the soil shear strength parameters. Under the condition of d = 0.5 mm, the variations of c'_r and φ'_r were different from each other. Compared with the unreinforced soil, the effective cohesions of the root-soil composites slightly increased for $\alpha = 30^\circ$ and $\alpha = 60^\circ$, while that of $\alpha = 0^\circ$ and $\alpha = 90^\circ$ significantly increased. Moreover, c'_r respectively increased by 11.7% ($\alpha = 60^\circ$), 22.2% ($\alpha = 30^\circ$), 32.6% ($\alpha = 0^\circ$), and 66.4% ($\alpha = 90^\circ$). Meanwhile, the variations of φ'_r were slight under all root distribution angles. Additionally, the effective internal friction angle of

the root-soil composites was lower than that of the unreinforced soil. φ_r' increased from 26.07° (α = 0°) to 26.66° (α = 60°), and then decreased to 26.22° (α = 90°).

Table 3. Strength parameters of unreinforced soils and root-soil composites.

Strength Parameter	Control Conditions												
	WR *	0.5 mm Root Diameter				1.0 mm Root Diameter				2.0 mm Root Diameter			
		0°	30°	60°	90°	0°	30°	60°	90°	0°	30°	60°	90°
c' (kPa)	30.17	40.00	36.88	33.70	50.21	45.43	42.14	38.99	60.27	51.92	48.64	43.03	74.15
$\Delta c'$ (kPa)	-	9.83	6.71	3.53	20.04	15.26	11.97	8.82	30.10	21.75	18.47	12.86	43.98
φ' (°)	26.69	26.07	26.12	26.66	26.22	26.96	26.69	26.93	26.77	26.87	27.07	27.26	26.85

* Without root.

Under the condition of d = 1.0 mm, the effective cohesion of the root-soil composites increased in the order of 60°, 30°, 0°, and 90° distribution angles and was greater than that of the unreinforced soil. c_r' increased by 50.6% for α = 0° and 99.8% for α = 90°. What is more, compared with the unreinforced soil, the effective internal friction angle of the root-soil composites slightly increased.

Under the condition of d = 2.0 mm, the effective cohesion of the root-soil composites increased greatly. The maximum increase of effective cohesion was 145.8% for α = 90°. c_r' respectively increased by 72.1% (α = 0°), 61.2% (α = 30°), and 42.6% (α = 60°). Compared with the unreinforced soil, φ_r' increased for all the root distribution angles. Although φ_r' increased, the maximum increase among all root distribution angles was only 2.1%.

According to the results, the root distribution angle and root diameter significantly influence the shear strength of soils. The effects of roots on the soil shear strength are mainly represented in the increase of the effective cohesion. Furthermore, roots have slight effects on the effective internal friction angle. The effective cohesion of the root-soil composites increases with the increase of the root diameter. With the increase of the root distribution angle, the effective cohesion of the root-soil composites first decreases, and then increases.

4.2. Root Reinforcement Coefficients

According to Equations (10) and (11), the root reinforcement coefficients (n and m) of the root-soil composites under different root distribution angles and diameters were obtained from the shear strength parameters of the root-soil composites (Table 3). The coefficients are listed in Table 4.

Table 4. Root reinforcement coefficients of unreinforced soils and root-soil composites.

Root Reinforcement Coefficient	Control Condition												
	WR *	0.5 mm Root Diameter				1.0 mm Root Diameter				2.0 mm Root Diameter			
		0°	30°	60°	90°	0°	30°	60°	90°	0°	30°	60°	90°
n	1.000	0.976	0.978	0.999	0.982	1.011	1.000	1.010	1.003	1.007	1.015	1.022	1.006
m	1.000	1.326	1.222	1.117	1.664	1.506	1.397	1.292	1.998	1.721	1.612	1.426	2.458

* Without root.

In Table 4, both of the root reinforcement coefficients of the unreinforced soil were 1.000 and the root reinforcement coefficients of the root-soil composites were different from each other.

The parameter n was less than 1.000 for the 0.5-mm-diameter root in the root-soil composites. Under the condition of the 1.0-mm-diameter root, n was more than 1.000 for the root distribution angles of 0°, 60°, and 90°, while n = 1.000 for the root distribution angle of 30°. Under the 2.0-mm-diameter root condition, the values of n were all more than 1.000 for the different root distribution angles. Regardless of diameter, m exceeded 1.000 for all root-soil composites and decreased in the order of 90°, 0°, 30°, and 60° of root distribution angles (α). Moreover, the maximum value of n was 1.022 and that of m was 2.458.

n represents the ratio of the passive earth pressure of the root-soil composite to that of the unreinforced soil. m describes the ratio of the effective cohesion of the root-soil composite to that of the unreinforced soil. Additionally, m increases with the increase of the root diameter. With the increase in the root distribution angle, m first decreases and then increases. However, the variations of n are slight.

4.3. Deformation Characteristics of the Soil Samples

The root had a significant impact on the sample deformation evolutions. Taking 0.5-mm-diameter root composites under a confining pressure of 50 kPa as an example, the deformation of these rooted soils was shown in Figure 3.

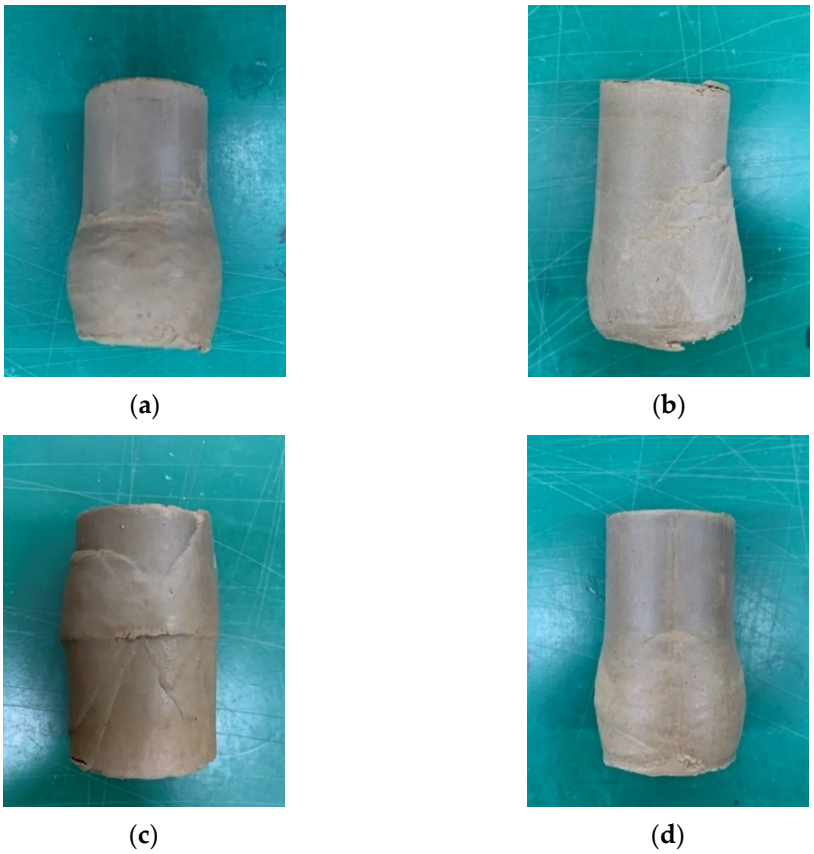

Figure 3. Deformation characteristics of root-soil composites under the 50-kPa confining pressure and 0.5-mm root diameter: (**a**) $\alpha = 0°$, (**b**) $\alpha = 30°$, (**c**) $\alpha = 60°$, and (**d**) $\alpha = 90°$.

Figure 3 shows the obvious axial and lateral deformation of all samples. In Figure 3a,d, there is no clear failure surface in the root-soil composites with obvious lateral deformation for the root distribution angle of 0° and 90°. Meanwhile, the lateral deformation rate was 13.1% for $\alpha = 0°$ and 10.9% for $\alpha = 90°$. In Figure 3b, the failure surface did not run through the whole sample with the run-through rate of 48.7% when $\alpha = 30°$. Additionally, the main lateral deformation rate was 14.9%. Figure 3c shows an obvious failure surface of the 60°-distribution-angle composite with a 79.5% run-through rate and lateral swelling (17.0% lateral deformation rate) which appeared in the middle of the sample. However, compared with the unreinforced soil, the development of the failure surface for the rooted soil samples was greatly restrained.

The addition of roots can significantly affect the deformation characteristics of the root-soil composites. Owing to the interaction between the roots and the soil particles, the roots can bear partial shear stress, and restrain the lateral deformation of the rooted soils. With the addition of the roots, the strength and stiffness of the root-soil composites increase.

5. Discussion

5.1. Effects of Root Distribution Angles

Table 3 shows that the shear strength of the root-soil composites was higher than that of the unreinforced soil, which is consistent with many previous studies [27,38,45,46]. Among the four root distribution angles (0°, 30°, 60°, and 90°), the shear strength of the rooted soils decreased in the order of 90°, 0°, 30°, and 60°. The shear strength of rooted soils increased by 2.5 times (α = 90°), 1.7 times (α = 0°), 1.6 times (α = 30°), and 1.4 times (α = 60°). When α = 90°, the roots had the strongest effect on the shear strength and were most conductive to resist the axial pressure of the root-soil composite. Thus, the shear strength of the rooted soils can be improved by the addition of roots.

According to the Mohr-Coulomb theory, the failure angle is $\alpha_f = 45^{\circ} + \varphi'/2$. When φ' = 26.69° for the unreinforced soil, α_f = 58.35° can be obtained. Therefore, α = 60° was closest to the failure angle of the soils (α_f). Meanwhile, only a small part of the roots passed through the failure surface of the soils and the soils were most prone to failure and the shear strength was the lowest. This finding is consistent with the results of Meng et al. [47]. The closer the root distribution angle is to the failure angle, the less the number of roots passing through the shear failure surface. When the root-soil composites are stressed, the tensile strength of the roots cannot be fully exerted. Therefore, the shear strength of the root-soil composites for α = 60° cannot be effectively enhanced by roots. When the root is vertically distributed, the roots can run through the failure surface of the soils, which can greatly improve the shear strength of the root-soil composites. Additionally, the lateral deformation of the root-soil composites is smaller than that of the unreinforced soils [48]. The constraint of the roots on the soil deformation depends on the tensile strength of the roots. The run-through rate and the lateral deformation rate of the root-soil composites increase in the order of 90°, 0°, 30°, and 60° root distribution angles. Moreover, the larger the run-through rate and lateral deformation rate of the soils are, the smaller the restraint and the shear strength of the soils are, and the easier the soils fail.

5.2. Effects of Root Diameter on the Root-Soil Composites

In Table 3, under the same root distribution angle, the shear strength of the root-soil composites increased with the increasing root diameter. When d = 0.5 mm, the shear strength of the root-soil composites increased by the smallest amount, which is related to the soil bonding failure and the small area of contact between roots and soils. This result agrees with the previous studies [47,49]. Additionally, the shear strength of rooted soil was enhanced by 1.7 times (d = 0.5 mm), 2.0 times (d = 1.0 mm), and 2.5 times (d = 2.0 mm).

The larger the diameter of roots, the greater the shear strength of root-soil composites and the stronger the effect of roots on the shear strength. Large diameter roots can increase the root-soil contact area, and a large area of contact between the roots and soils means an increase in the frictional strength between the root-soil interface [50]. Therefore, the shear strength of the rooted soils is enhanced. Additionally, the larger the root diameter, the greater the force required for root fracture [51]. Thus, the large diameter roots are not easy to fail and the soils can be greatly reinforced. Moreover, the surface of large diameter roots is rougher than that of small diameter roots. With the increase in the root diameter, the soils around the roots are subjected to the root radial force and become relatively dense, which leads to greater friction between the root-soil interface [52]. Meanwhile, the binding force between the soil particles around the roots increases. Thus, the shear strength of the root-soil composites increases.

5.3. Variations of the Root Reinforcement Coefficients

Equation (2) is equivalent to Equation (12) when both n and m are 1.000. The result shows that Equation (12) is a generalized limit equilibrium equation for all kinds of soils. The limit equilibrium equation for the unreinforced soil is only a particular case.

In Figures 4 and 5, the variation in m is consistent with that of c', and changes of n are similar to that of φ'. Variations in root reinforcement coefficients directly describe the

effects of the root distribution angle and root diameter on the shear strength parameters of the root-soil composites. In Table 3, the main contribution of roots to soil shear strength was to increase the effective cohesion. The internal friction angle is mainly affected by the soil particle structure [53]. However, compared with soil mass, the root content (0.15%) of the root-soil composites is small. Therefore, the effective internal frictional angle of the rooted soil had a slight change [36,54].

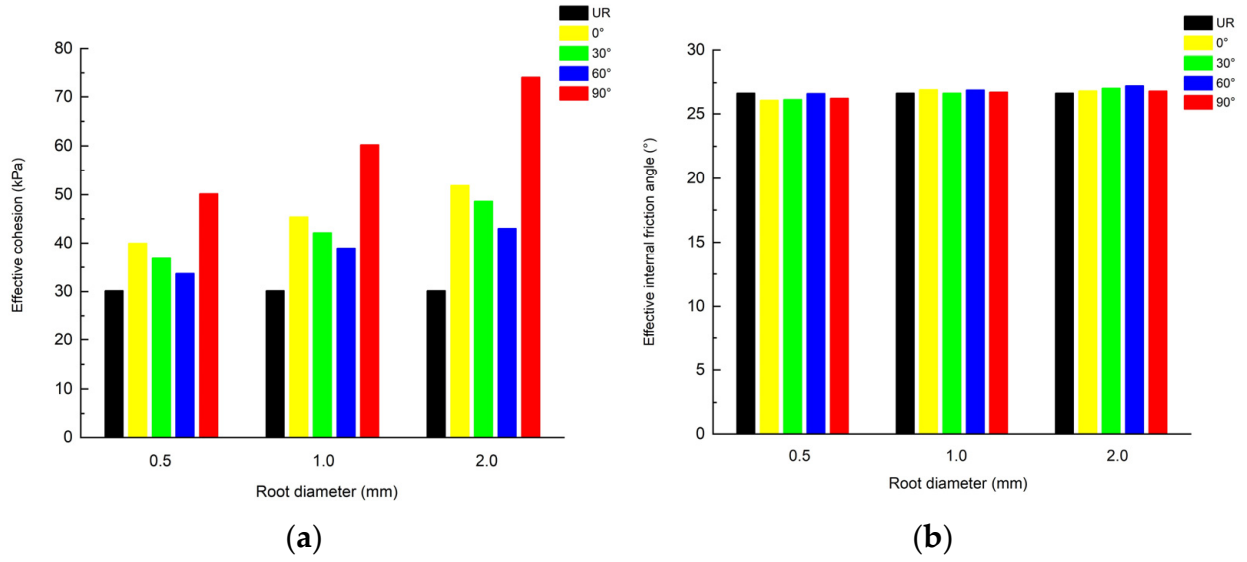

Figure 4. Variations of soil shear strength parameters under different conditions: (**a**) c' and (**b**) φ'.

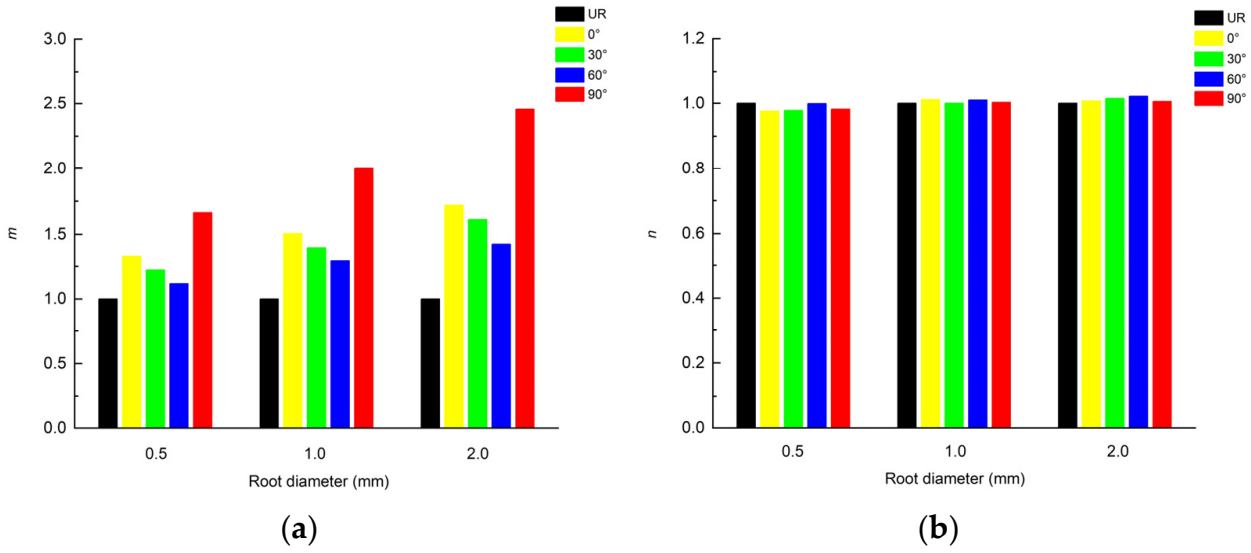

Figure 5. Variations of the soil root reinforcement coefficient under different conditions: (**a**) m, and (**b**) n.

When the increments of the effective cohesion and the effective internal frictional angle ($\Delta c'$ and $\Delta\varphi'$) were both greater than zero, n and m were greater than 1.000. When $\Delta c'$ was greater than zero, m was more than 1.000. While $\Delta\varphi'$ was less than zero, n was less than 1.000. Furthermore, n and m were not generally equal to 1.000.

There are two different conditions, as shown in Figure 6. τ and τ_l denote the shear strength of the unreinforced soil and the root-soil composites, respectively. Considering the root distribution angles and the root diameters, there are several shear strength envelope relationships of the unreinforced soil and the root-soil composites. In Figure 6a, when $m = 1.426$ and $n = 1.002$, meaning that $\Delta c' > 0$ and $\Delta\varphi' > 0$, the shear strength envelopes of the root-soil composites are commonly larger than the shear strength envelope of the

unreinforced soil. Figure 6a presents the envelopes of the shear strength of $\alpha = 60^\circ$ under $d = 2.0$ mm. Figure 6b presents the envelopes for a 0.5-mm-diameter-root composite with $\alpha = 0^\circ$. In Figure 6b, when $m = 1.326$ and $n = 0.978$ (i.e., $\Delta c' > 0$ and $\Delta\varphi' < 0$), the shear strength envelope of the root-soil composites is smaller than that of the unreinforced soil. Additionally, Figure 6 demonstrates that the changes of the root reinforcement coefficients affect the failure principal stress of the root-soil composites. The failure principal stress of the root-soil composites decreases with decreasing n and m.

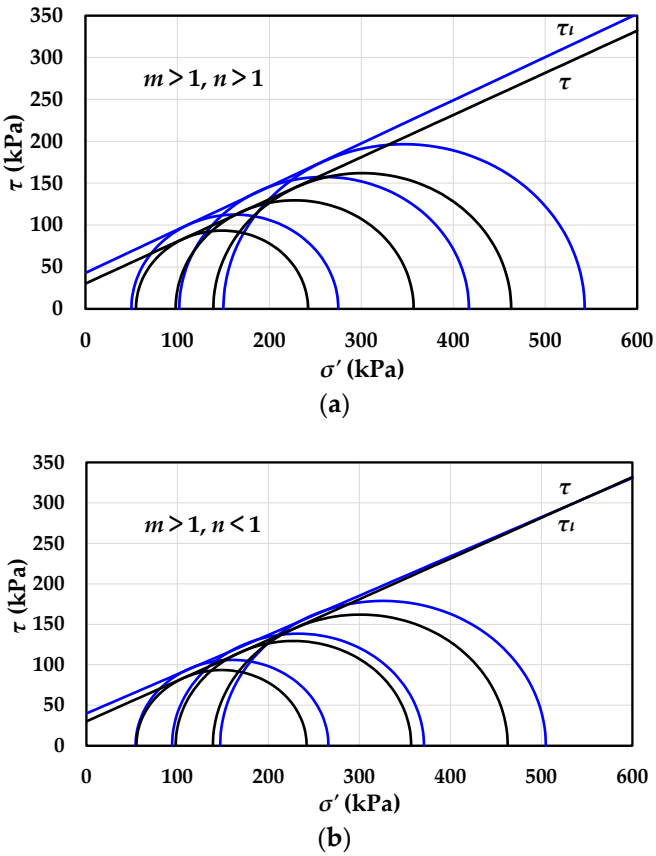

Figure 6. Shear strength envelope diagrams for unreinforced soil and root-soil composites: (**a**) $m = 1.426$, $n = 1.002$, (**b**) $m = 1.326$, $n = 0.978$.

5.4. Root Reinforcement Mechanism

The interaction between roots and soils can increase the mechanical properties and shear strength of soils, thus increasing the stability of slopes [36]. The exertion of the root tensile strength depends on the friction between the root-soil interface. Therefore, enhancing the friction between the root-soil interface is key to improve the shear strength of the root-soil composites.

Compared with soils, plant roots have a strong tensile strength, which can offset a part of the shear stress. Under loading, the deformation of the root-soil composites causes the relative displacement and mutual dislocation between roots and soils, which can generate the friction between the root-soil interface. The tensile property of plant roots can be combined with the compressive property of soils through the friction between the root-soil interface [52]. Roots can effectively improve the shear strength of soils, and enhance the capacity of soils to resist the shear failure. On the one hand, the increase of the root diameter can enlarge the root-soil contact area, root surface roughness, and the compactness of soils around roots, which is beneficial to improve the friction on the root-soil interface. On the other hand, the root distribution angle affects the number of plant roots passing through the shear failure surface of soils, thus impacting the enhancement of roots on the shear strength of rooted soils. The more the number of roots passing through the shear failure

surface, the stronger the transmission and dispersion effect of roots on the soil stress, and the greater the shear strength of the rooted soils.

In general, the greater the shear strength of the rooted soils, the higher the slope stability [55]. According to the results of this study, the shear strength of the rooted soils increases with an increasing root diameter, and the vertical root distribution pattern can greatly enhance the shear strength of root-soil composites. Thus, plants with a larger root diameter and mainly 90° root distribution angle are suggested to reinforce slopes.

6. Conclusions

The following conclusions are drawn from the results of the study.

1. Root distribution angles and root diameters affect the shear strengths of the root-soil composites and the shear strength of rooted soils is enhanced by 1.1–2.5 times. The shear strength of the root-soil composites becomes high in the order of 60°, 30°, 0°, and 90° distribution angles, and decreases in the order of 2.0 mm, 1.0 mm, and 0.5 mm root diameters. Moreover, roots mainly affect the effective cohesion of the soils. However, the effective internal friction angle of the rooted soils changes slightly.
2. The run-through rate and the lateral deformation of the root-soil composites increase in the order of 90°, 0°, 30°, and 60° root distribution angles (α), and the run-through rate of $\alpha = 90°$ and $\alpha = 0°$ are both 0. Meanwhile, the lateral deformation rate declines from 17.0% for $\alpha = 60°$ to 10.9% for $\alpha = 90°$. Roots can effectively restrain the deformation of the root-soil composites.
3. Two root reinforcement coefficients n and m were proposed to develop the limit equilibrium equation of the root-soil composites. n and m can be calculated by φ' and c'. The limit equilibrium of the unreinforced soil is equivalent to that of the root-soil composite when both n and m are 1.000, which means that the limit equilibrium equation of the unreinforced soil is only a particular case. Therefore, the limit equilibrium equation of the root-soil composites has a wide applicability. Additionally, n and m represent the effects of root distribution angles and root diameters on the failure principal stress of the root-soil composites, respectively. The failure principal stress of the root-soil composites is positively correlated with n and m.

Author Contributions: P.L. and L.W. conceived and designed the experiments; L.W. and X.L. guided the experiment; P.L. performed the experiments and analyzed the data; P.L., L.W., X.L., H.Z. and J.Z. wrote the manuscript; P.L., X.X., L.W., X.L., H.Z. and J.Z. contributed critically to improve the manuscript. All authors have read and agreed to the published version of the manuscript.

Funding: This research was funded by the National Natural Science Foundations of China (Grant No. 41790432, Project leader: Peng Cui).

Institutional Review Board Statement: Not applicable.

Informed Consent Statement: Not applicable.

Data Availability Statement: Not applicable.

Conflicts of Interest: The authors declare no conflict of interest.

Notation

τ_f	Shear strength
σ	Normal stress
u	Pore water pressure
σ'	Effective stress
c'	Effective cohesion
φ'	Effective internal friction angle
σ_3	Confining pressure
σ_1	Failure principal stress of the unreinforced soil
σ_{1l}	Failure principal stress of the root-soil composite

K_p	Passive earth pressure coefficient of the unreinforced soil
K_{pl}	Passive earth pressure coefficient of the root-soil composite
c'_{us}	Effective cohesion of the unreinforced soil
φ'_{us}	Effective internal frictional angle of the unreinforced soil
c'_{rs}	Effective cohesion of the root-soil composite
φ'_{rs}	Effective internal frictional angle of the root-soil composite
$\Delta\sigma_{1l}$	Deviator of the failure principal stress of the unreinforced soil and root-soil composite
$\Delta\sigma_{3g}$	Generalized equivalent confining pressure
n, m	Root reinforcement coefficients of the soil

References

1. Kim, D.H.; Gratchev, I.; Balasubramaniam, A. Determination of joint roughness coefficient (JRC) for slope stability analysis: A case study from the Gold Coast area, Australia. *Landslides* **2013**, *10*, 657–664. [CrossRef]
2. Wu, L.Z.; Selvadurai, A.P.S.; Zhang, L.M.; Huang, R.Q.; Huang, J.S. Poro-mechanical coupling influences on potential for rainfall-induced shallow landslides in unsaturated soils. *Adv. Water Resour.* **2016**, *98*, 114–121. [CrossRef]
3. Lin, F.; Wu, L.Z.; Huang, R.Q.; Zhang, H. Formation and characteristics of the Xiaoba landslide in Fuquan, Guizhou, China. *Landslides* **2018**, *15*, 669–681. [CrossRef]
4. Wu, L.Z.; Li, S.H.; Huang, R.Q.; Xu, Q. A new grey prediction model and its application to predicting landslide displacement. *Appl. Soft. Comput.* **2020**, *95*, 106543. [CrossRef]
5. Li, S.H.; Luo, X.H.; Wu, L.Z. A new method for calculating failure probability of landslide based on ANN and convex set model. *Landslides* **2021**, *18*, 2855–2867. [CrossRef]
6. Zhu, S.R.; Wu, L.Z.; Huang, J.S. Application of an improved P(m)-SOR iteration method for flow in partially saturated soils. *Comput. Geosci.* **2022**, *26*, 131–145. [CrossRef]
7. Zhu, S.R.; Wu, L.Z.; Song, X.L. An improved matrix split-iteration method for analyzing underground water flow. *Eng. Comput.* **2022**, Online. [CrossRef]
8. Montagnoli, A.; Terzaghi, M.; Magatti, G.; Scippa, G.S.; Chiatante, D. Conversion from coppice to high stand increase soil erosion in steep forestland of European beech. *Reforesta* **2016**, *2*, 60–75. [CrossRef]
9. Zegeye, A.D.; Langendoen, E.J.; Tilahun, S.A.; Mekuria, W.; Poesen, J.; Steenhuis, T.S. Root reinforcement to soils provided by common Ethiopian highland plants for gully erosion control. *Ecohydrology* **2018**, *11*, 1940–1951. [CrossRef]
10. Mitsch, W.J. Ecological engineering—The 7-year itch. *Ecol. Eng.* **1998**, *10*, 119–138. [CrossRef]
11. Osman, N.; Barakbah, S.S. Parameters to predict slope stability—Soil water and root profiles. *Ecol. Eng.* **2006**, *28*, 90–95. [CrossRef]
12. Wu, T.H. Root reinforcement of soil: Review of analytical models, test results, and applications to design. *Can. Geotech. J.* **2013**, *50*, 259–274. [CrossRef]
13. Ai, X.Y.; Wang, L.; Xu, D.P.; Rong, J.J.; Ai, S.H.; Liu, S.; Li, C.L.; Ai, Y.W. Stability of artificial soil aggregates for cut slope restoration: A case study from the subalpine zone of southwest China. *Soil Till. Res.* **2021**, *209*, 104934. [CrossRef]
14. Li, S.H.; Cui, P.; Cheng, P.; Wu, L.Z. Modified Green–Ampt Model considering vegetation root effect and redistribution characteristics for slope stability analysis. *Water Resour. Manag.* **2022**, *36*, 2395–2410. [CrossRef]
15. McGuire, L.A.; Rengers, F.K.; Kean, J.W.; Coe, J.A.; Mirus, B.B.; Baum, R.L.; Godt, J.W. Elucidating the role of vegetation in the initiation of rainfall-induced shallow landslides: Insights from an extreme rainfall event in the Colorado Front Range. *Geophys. Res. Lett.* **2016**, *43*, 9084–9092. [CrossRef]
16. Gonzalez-Ollauri, A.; Mickovski, S.B. Plant-soil reinforcement response under different soil hydrological regimes. *Geoderma* **2017**, *285*, 141–150. [CrossRef]
17. Feng, S.; Liu, H.W.; Ng, C.W.W. Analytical analysis of the mechanical and hydrological effects of vegetation on shallow slope stability. *Comput. Geotech.* **2020**, *118*, 103335. [CrossRef]
18. Löbmann, M.T.; Geitner, C.; Wellstein, C.; Zerbe, S. The influence of herbaceous vegetation on slope stability-A review. *Earth-Sci. Rev.* **2020**, *209*, 103328. [CrossRef]
19. Zhu, H.; Zhang, L.M.; Garg, A. Investigating plant transpiration-induced soil suction affected by root morphology and root depth. *Comput. Geotech.* **2018**, *103*, 26–31. [CrossRef]
20. Yildiz, A.; Graf, F.; Rickli, C.; Springman, S.M. Assessment of plant-induced suction and its effects on the shear strength of rooted soils. *Geotech. Eng.* **2019**, *172*, 507–519. [CrossRef]
21. Liu, H.W.; Feng, S.; Ng, C.W.W. Analytical analysis of hydraulic effect of vegetation on shallow slope stability with different root architectures. *Comput. Geotech.* **2016**, *80*, 115–120. [CrossRef]
22. Ng, C.W.W.; Zhang, Q.; Ni, J.J.; Li, Z.Y. A new three-dimensional theoretical model for analysing the stability of vegetated slopes with different root architectures and planting patterns. *Comput. Geotech.* **2021**, *130*, 103912. [CrossRef]
23. Su, X.M.; Zhou, Z.C.; Liu, J.E.; Cao, L.G.; Liu, J.Y.; Wang, P.P. Estimating slope stability by the root reinforcement mechanism of Artemisia sacrorum on the Loess Plateau of China. *Ecol. Model* **2021**, *444*, 109473. [CrossRef]
24. Jiang, K.Y.; Chen, L.H.; Gai, X.G.; Yang, W.J. Relationship between tensile properties and microstructures of three different broadleaf tree roots in North China. *Trans. Chin. Soc. Agric. Eng.* **2013**, *29*, 115–123. (In Chinese)

25. Zhang, C.B.; Chen, L.H.; Liu, Y.P.; Ji, X.D.; Liu, X.P. Triaxial compression test of soil-root composites to evaluate influence of roots on soil shear strength. *Ecol. Eng.* **2010**, *36*, 19–26. [CrossRef]
26. Wu, T.H. *Investigation of Landslides on Prince of Wales Island, Alaska*; Geotechnical Engineering Report 5; Department of Civil Engineering, Ohio State University: Columbus, OH, USA, 1976.
27. Waldron, L.J. The shear resistance of root-permeated homogeneous and stratified soil. *Soil Sci. Soc. Am. J.* **1977**, *41*, 843–849. [CrossRef]
28. Wu, T.H.; McKinell, W.P.; Swanston, D.N. Strength of tree roots and landslides on Prince of Wales Island, Alaska. *Can. Geotech. J.* **1979**, *16*, 19–33. [CrossRef]
29. Gray, D.H.; Sotir, R.B. Biotechnical and soil bioengineering slope stabilization: A practical guide for erosion control. *Soil Sci.* **1998**, *163*, 83–85. [CrossRef]
30. Pollen, N.; Simon, A. Estimating the mechanical effects of riparian vegetation on stream bank stability using a fiber bundle model. *Water Resour. Res.* **2005**, *41*, 226–244. [CrossRef]
31. Schwarz, M.; Preti, F.; Giadrossich, F.; Lehmann, P.; Or, D. Quantifying the role of vegetation in slope stability: A case study in Tuscany (Italy). *Ecol. Eng.* **2010**, *36*, 285–291. [CrossRef]
32. Satyanaga, A.; Rahardjo, H. Stability of unsaturated soil slopes covered with Melastoma malabathricum in Singapore. *Proc. Inst. Civ. Eng.-Geotech. Eng.* **2019**, *172*, 530–540. [CrossRef]
33. Rahardjo, H.; Satyanaga, A.; Wang, C.L.; Wong, J.L.H.; Lim, V.H. Effects of unsaturated properties on stability of slope covered with Caesalpinia Crista in Singapore. *Environ. Geotech.* **2020**, *7*, 393–403. [CrossRef]
34. Zhou, Y.Y.; Wang, X.M. Mesomechanics characteristics of soil reinforcement by plant roots. *Bull. Eng. Geol. Environ.* **2019**, *78*, 3719–3728. [CrossRef]
35. Zhang, C.B.; Chen, L.H.; Jiang, J. Vertical root distribution and root cohesion of typical tree species on the Loess Plateau, China. *J. Arid. Land* **2014**, *6*, 601–611. [CrossRef]
36. Lian, B.Q.; Peng, J.B.; Zhan, H.B.; Wang, X.G. Mechanical response of root-reinforced loess with various water contents. *Soil Till. Res.* **2019**, *193*, 85–94. [CrossRef]
37. Guo, P.; Xia, Z.; Liu, Q.; Xiao, H.; Gao, F.; Zhang, L.; Li, M.Y.; Yang, Y.S.; Xu, W.N. The mechanism of the plant roots' soil-reinforcement based on generalized equivalent confining pressure. *PeerJ* **2020**, *8*, e10064. [CrossRef]
38. Liu, Y.B.; Hu, X.S.; Yu, D.M.; Zhu, H.L.; Li, G.R. Influence of the roots of mixed-planting species on the shear strength of saline loess soil. *J. Mt. Sci.* **2021**, *18*, 806–818. [CrossRef]
39. *ASTM (D4287-11)*; Standard Practice for Classification of Soils for Engineering Purpose (Unified Soil Classification System). ASTM International: West Conshohocken, PA, USA, 2006.
40. *ASTM. (D854-02)*; Standard Test Methods for Specific Gravity of Soil Solids by Water Pycnometer. Annual Book of ASTM Standards. ASTM International: West Conshohocken, PA, USA, 2002.
41. *ASTM. (D4318-00)*; Standard Test Methods for Liquid Limit, Plastic Limit and Plasticity Index of Soils. Annual Book of ASTM Standards. ASTM International: West Conshohocken, PA, USA, 2000.
42. Li, Y.P.; Wang, Y.Q.; Ma, C.; Zhang, H.L.; Wang, Y.J.; Song, S.S.; Zhu, J.Q. Influence of the spatial layout of plant roots on slope stability. *Ecol. Eng.* **2016**, *91*, 477–486. [CrossRef]
43. Gyssels, G.; Poesen, J.; Bochet, E.; Li, Y. Impact of plant roots on the resistance of soils to erosion by water: A review. *Prog. Phys. Geogr.* **2005**, *29*, 189–217. [CrossRef]
44. Alam, S.; Banjara, A.; Wang, J.; Patterson, W.B.; Baral, S. Novel approach in sampling and tensile strength evaluation of roots to enhance soil for preventing erosion. *Open J. Soil Sci.* **2018**, *8*, 330–349. [CrossRef]
45. Cazzuffi, D.; Crippa, E. Shear strength behaviour of cohesive soils reinforced with vegetation. In Proceedings of the 16th International Conference on Soil Mechanics and Geotechnical Engineering: Geotechnology in Harmony with the Global Environment, Osaka, Japan, 12 September 2005.
46. Fan, C.C.; Su, F. Role of roots in the shear strength of root-reinforced soils with high moisture content. *Ecol. Eng.* **2008**, *33*, 157–166. [CrossRef]
47. Meng, S.Y.; Zhao, G.Q.; Yang, Y.Y. Impact of plant root morphology on rooted-soil shear resistance using triaxial testing. *Adv. Civ. Eng.* **2020**, *2020*, 8825828. [CrossRef]
48. Tan, H.M.; Chen, F.M.; Chen, J.; Gao, Y.F. Direct shear tests of shear strength of soils reinforced by geomats and plant roots. *Geotext Geomembr.* **2019**, *47*, 780–791. [CrossRef]
49. Schmidt, K.M.; Roering, J.J.; Stock, J.D.; Dietrich, W.E.; Montgomery, D.R.; Schaub, T. The variability of root cohesion as an influence on shallow landslide susceptibility in the Oregon Coast Range. *Can. Geotech. J.* **2001**, *38*, 995–1024. [CrossRef]
50. Ji, X.D.; Cong, X.; Dai, X.Q.; Zhang, A.; Chen, L.H. Studying the mechanical properties of the soil-root interface using the pullout test method. *J. Mt. Sci.* **2018**, *15*, 882–893. [CrossRef]
51. Vergani, C.; Chiaradia, E.A.; Bischetti, G.B. Variability in the tensile resistance of roots in Alpine forest tree species. *Ecol. Eng.* **2012**, *46*, 43–56. [CrossRef]
52. Su, L.J.; Hu, B.L.; Xie, Q.J.; Yu, F.W.; Zhang, C.L. Experimental and theoretical study of mechanical properties of root-soil interface for slope protection. *J. Mt. Sci.* **2020**, *17*, 2784–2795. [CrossRef]
53. Rasti, A.; Adarmanabadi, H.R.; Pineda, M.; Reinikainen, J. Evaluating the effect of soil particle characterization on internal friction angle. *Am. J. Eng. Appl. Sci.* **2021**, *14*, 129–138. [CrossRef]

54. Normaniza, O.; Faisal, H.A.; Barakbah, S.S. Engineering properties of Leucaena leucocephala for prevention of slope failure. *Ecol. Eng.* **2008**, *32*, 215–221. [CrossRef]
55. Hu, X.S.; Brierley, G.; Zhu, H.L.; Li, G.R.; Fu, J.T.; Mao, X.Q.; Yu, Q.Q.; Qiao, N. An exploratory analysis of vegetation strategies to reduce shallow landslide activity on loess hillslopes, Northeast Qinghai-Tibet Plateau, China. *J. Mt. Sci.* **2013**, *10*, 668–686. [CrossRef]